

# The Photometric Properties of Isolated Early-Type Galaxies

Fatma M. Reda<sup>1,2\*</sup> Duncan A. Forbes<sup>1†</sup> Michael A. Beasley<sup>1,3‡</sup>  
 Ewan J. O’Sullivan<sup>4§</sup> Paul Goudfrooij<sup>5¶</sup>

<sup>1</sup>Centre for Astrophysics & Supercomputing, Swinburne University, Hawthorn, VIC 3122, Australia

<sup>2</sup>Astronomy Department, National Research Institute of Astronomy and Geophysics, Helwan, Cairo 11421, Egypt

<sup>3</sup>Lick Observatory, University of California, Santa Cruz, CA 95064, USA

<sup>4</sup>Harvard-Smithsonian Center for Astrophysics, MS-67, 60 Garden Street, Cambridge, MA 02138, USA

<sup>5</sup>Space Telescope Science Institute, 3700 San Martin Drive, Baltimore, MD 21218, USA

Accepted 2004 July 21. Received 2004 June 19

## ABSTRACT

Isolated galaxies are important since they probe the lowest density regimes inhabited by galaxies. We define a sample of 36 nearby isolated early-type galaxies for further study. Our isolation criteria require them to have no comparable-mass neighbours within 2  $B$ -band magnitudes, 0.67 Mpc in the plane of the sky and  $700 \text{ km s}^{-1}$  in recession velocity. New wide-field optical imaging of 10 isolated galaxies with the Anglo-Australian Telescope confirms their early-type morphology and relative isolation. We also present imaging of 4 galaxy groups as a control sample. The isolated galaxies are shown to be more gravitationally isolated than the group galaxies. We find that the isolated early-type galaxies have a mean effective colour of  $(B-R)_e = 1.54 \pm 0.14$ , similar to their high-density counterparts. They reveal a similar colour-magnitude relation slope and small intrinsic scatter to cluster ellipticals. They also follow the Kormendy relation of surface brightness versus size for luminous cluster galaxies. Such properties suggest that the isolated galaxies formed at a similar epoch to cluster galaxies, such that the bulk of their stars are very old. However, our galaxy modelling reveals evidence for dust lanes, plumes, shells, boxy and disk isophotes in four out of nine galaxies. Thus at least some isolated galaxies have experienced a recent merger/accretion event which may have induced a small burst of star formation. We derive luminosity functions for the isolated galaxies and find a faint slope of  $-1.2$ , which is similar to the ‘universal’ slope found in a wide variety of environments. We examine the number density distribution of galaxies in the field of the isolated galaxies. Only the very faintest dwarf galaxies ( $M_R \gtrsim -15.5$ ) appear to be associated with the isolated galaxies, whereas any intermediate-luminosity galaxies appear to lie in the background. Finally we discuss possible formation scenarios for isolated early-type galaxies. Early epoch formation and a merger/accretion of galaxies are possible explanations. The collapse of a large, virialised group is an unlikely explanation, but that of a poor group remains viable.

**Key words:** galaxies: elliptical and lenticular - galaxies: photometry - galaxies: structure - galaxies: luminosity function, mass function.

## 1 INTRODUCTION

Early-type galaxies are more commonly found in dense environments such as clusters and groups, than in the field. Within a cluster, the dense core regions are richer with early-type galaxies than the lower-density outskirts. This distribution of galaxy morphology with environment is known as the morphology-density relation (Dressler 1980). In all environments, early-type galaxies show morphological fine struc-

\* freda@astro.swin.edu.au

† dforbes@swin.edu.au

‡ mbeasley@ucolick.org

§ ejos@head-cfa.cfa.harvard.edu

¶ goudfrooij@stsci.edu

tures such as tidal tails, shells, dust lanes, disk or boxy components, etc. (e.g. Schweizer et al. 1990). Theoretical models often attempt to explain these morphological structures as a result of past merging in earlier galaxy formation stages or, alternatively, of tidal interactions with close neighbours. In dense cluster environments, merging was more likely at earlier epochs when the cluster was still forming and velocity dispersions were low enough to allow outright mergers.

Studies of the stellar populations in early-type galaxies in different environments suggest that field galaxies tend to be bluer, and have spectral indices indicating slightly younger mean stellar ages than their cluster counterparts (e.g. De Carvalho & Djorgovski 1992; Terlevich & Forbes 2002; Girardi et al. 2003). For a sample of 35 field early-type galaxies at a median redshift of 0.9, Kodama, Bower & Bell (1999) found some of them to be redder in their colour-magnitude relation (CMR) than that for Coma cluster galaxies. These authors concluded that at least half of the field early-type galaxies at these redshifts formed their stars at  $z > 2$ . The Kodama et al. sample of high redshift field galaxies shows a greater scatter in the CMR than that obtained by Stanford, Eisenhardt & Dickinson (1998) for a cluster at  $z \sim 0.9$ . This suggests a slightly more extended star formation period for early-type galaxies in the field than in clusters.

Isolated galaxies represent the ‘extreme field’ galaxy population and thus provide additional insight to those environment related processes. A carefully selected sample of isolated early-type galaxies will offer a useful tool to tackle many of the outstanding issues in galaxy formation. For example, in dense environments, separating the effects of secular and environmental evolution (“nature versus nurture”) is challenging. However, in such extremely low-density environments as those of isolated galaxies, one can eliminate the interaction processes that affect the evolution of galaxies in high-density environments such as ram-pressure stripping (Gunn & Gott 1972), strangulation (Balogh & Morris 2000; Fujita 2004), high-speed galaxy-galaxy encounters and tidal interactions with the cluster gravitational potential (Moore et al. 1996, 1999; Moore, Lake & Katz 1998). Previous studies such as Karachentseva (1973), Colbert, Mulchaey & Zabludoff (2001), Aars, Marcum & Fanelli (2001), Kuntschner et al. (2002), Smith & Martinez (2003) and Stocke et al. (2004) have introduced samples of early-type galaxies that are in low-density environments or are isolated from neighbours. Each study has its own advantages and limitations. In this paper, we define a new sample of 36 candidate isolated early-type galaxies with strict isolation conditions to ensure the absence of any strong tidal effects from a massive neighbour. Using the Wide Field Imager (WFI) on the 3.9-m Anglo-Australian Telescope (AAT) we obtained imaging in the  $B$  and  $R$  filters for a wide area surrounding 10 galaxies in the sample. This allows us to study the galaxy surface density distribution and photometric parameters of the faint galaxies in these fields.

In section 2, we give a summary of the previous studies of isolated early-type galaxies stating their selection criterion and briefly mention their results. Our selection criteria and the sample candidates are presented in section 3. Observations and data reduction for a subsample of 10 isolated galaxies and a comparison sample, are discussed in section 4, while their photometric measurements as well as mod-

elling, residual images and isophotal shape parameters are discussed in section 5. The detections of galaxies in the field are presented in section 6. Finally, we discuss the results and possible formation scenarios for isolated early-type galaxies in section 7. Throughout this paper we assume a Hubble constant of  $H_0 = 75 \text{ km s}^{-1} \text{ Mpc}^{-1}$ .

## 2 PREVIOUS STUDIES OF ISOLATED GALAXIES

Here we briefly review previous studies of galaxies in low density environments. Each study had its own advantages and limitations.

*Karachentseva (1973)* - a catalogue of  $\sim 1000$  galaxies with  $m_B < 15.7$  and declination  $> -3^\circ$ . The catalogue was chosen from the Zwicky et al. (1957) catalogue which is known to be biased against low surface brightness galaxies. The environment of each galaxy was inspected using the Palomar Observatory Sky Survey (POSS) for large neighbours. Isolation was established as the absence of companions within 20 galaxy diameters that have less than a  $\pm 2$  magnitude difference from the primary galaxy (Stocke et al. 2004). Due to saturation, poor resolution or other reasons in the POSS plates, one half of ellipticals in this catalogue appear to be misclassified (Saucedo-Morales & Bieging 2001).

*Reduzzi, Longhetti & Rampazzo (1996)* - a sample of 61 galaxies was selected from ‘The Surface Photometry Catalogue’ of the ESO-Uppsala Galaxies survey (Lauberts & Valentijn 1989). The galaxies were considered as isolated when the average number of galaxies of any morphology type was  $\leq 1.5$  within a radius of  $1^\circ$ . The sample of 61 galaxies were imaged for 20 min each at the 0.9-m ESO-Dutch telescope at La Silla, Chile. They noted that ten of the galaxies (i.e., 16% of their galaxy sample) contained spiral arms or bars, indicating they were of late-type morphology. The isolation of the galaxies was quantified using the ratio of the separation between the target and the nearest galaxy in units of the target galaxy diameter, i.e.  $S/D_{25}$ . For galaxies with  $S/D_{25} \leq 20$ , they examined an additional parameter, i.e. the luminosity ratio between the target and the nearest galaxy  $L_B/L_B^n$ . Using these two parameters  $S/D_{25}$  and  $L_B/L_B^n$ , they suggested that three galaxies had significant companions. One of these was a misclassified spiral. Based on the  $S/D_{25}$  and  $L_B/L_B^n$  values given in their paper, we determined that another 7 galaxies have significant companions. This leaves a total of 42 galaxies that can be considered isolated and of early-type. For their total sample of 61 galaxies, they found about 40% to have fine structures such as shells, dust, tidal tails, etc. Considering only the 42 isolated early-type galaxies, this percentage increases to 52%.

*Colbert, Mulchaey & Zabludoff (2001)* - a sample of 30 early-type galaxies, selected from the Third Reference Catalog (RC3; de Vaucouleurs et al. 1991) catalogue. Galaxies were selected to have no catalogued neighbours within  $1 h_{100}^{-1} \text{ Mpc}$  and  $\pm 1000 \text{ km s}^{-1}$ . Imaging of fields surrounding each galaxy was then used to confirm the lack of large galaxies within  $200 h_{100}^{-1} \text{ kpc}$ . However, some of the target galaxies themselves had luminosities only slightly greater than the catalogue limit. This means that some candidate isolated galaxies actually have nearby neighbours of quite similar lu-

minosity. Our examination of this sample with the Digitized Sky Survey (DSS) suggests that  $\sim 50\%$  of the candidate isolated galaxies have nearby neighbours.

*Aars, Marcum & Fanelli (2001)* - a sample of nine isolated elliptical galaxies selected from Karachentseva (1973). Two selection criteria were adopted for the initial identification of the isolated elliptical candidates. Firstly, elliptical galaxies were selected from the NASA Extragalactic Database (NED) that have separations of 2.5 Mpc from any other galaxy in the RC3. Secondly, the galaxy should have no neighbours with a known redshift (from NED) brighter than  $M_V = -16.5$ , within a projected separation of 2.5 Mpc. Only one galaxy in the RC3 and 13 in the Karachentseva (1973) catalogue meet these isolation criteria. From this sample of 14 galaxies, wide-field CCD images in the  $V$ -band were obtained using the 2.1-m telescope at McDonald Observatory. The one RC3 galaxy was a southern object which could not be imaged from McDonald Observatory and was therefore not included in the final sample. The images were used to check the isolation of these galaxies and to confirm the morphological type. This process identified that three were actually spiral galaxies and one was an irregular-type galaxy. These were excluded from further study leaving a final sample of nine isolated elliptical galaxies. Aars et al. defined a characteristic number density of projected galaxies on the sky for known loose groups and clusters. Comparing the number density of galaxies detected in the field of their 9 galaxies with these characteristic densities, they identified 5 galaxies to be in environments similar to those of loose groups. The environments of the remaining four galaxies were confirmed to be of low density.

*Kuntschner et al. (2002)* - a sample of nine nearby early-type galaxies in low-density environments (strictly speaking this is not an isolated galaxy sample). They were selected from the Hydra-Centaurus Catalogue of Raychaudhury (1989, 1990) to be early-type ( $T < -3$ ) with velocities  $< 7,000 \text{ km s}^{-1}$  and apparent magnitudes of  $b_J \leq 16.1$ . Their sample completeness at this magnitude is  $\sim 50\%$ . These galaxies were then required to have a maximum of two neighbours with  $b_J \leq 16.7$ , within a radius of 1.3 Mpc and a velocity difference  $350 \text{ km s}^{-1}$ . The result was a sample of 40 E and S0 galaxies. Visual inspection of the DSS images revealed that some of the galaxies have late-type morphologies leaving a sample of 30 early-type galaxies in low-density environments. Spectroscopic observations of 24 galaxies of this sample were obtained at the 2.3-m telescope at the Siding Spring Observatory, Australia. Kuntschner et al. found 5 galaxies to have emission line spectra typical of spiral galaxies, 3 have red shifts beyond  $7,000 \text{ km s}^{-1}$  (the adopted redshift limit in their work), 4 galaxies were classified as group/cluster members and 2 had spectra of poor signal-to-noise. Kuntschner et al. also obtained optical  $UV$  and near-infrared  $K_s$  imaging data for their sample with the CTIO 1.5-m telescope in Chile. By inspecting the model-subtracted images of the sample, one galaxy showed clearly visible spiral arms. In their final sample of 9 galaxies, 6 are members of the Arp & Madore (1987) catalogue of peculiar galaxies, i.e. they have indications of a past merger. The spectra indicate the presence of young stellar populations in several of these galaxies.

*Smith, Martinez & Graham (2003)* - a sample of 32 isolated early-type galaxies ( $T < -4$ ). The Lyon-Meudon Ex-

tragalactic Data Archive (LEDA) catalogue was used to find ellipticals which have velocities  $< 10,000 \text{ km s}^{-1}$ , absolute magnitudes  $M_B \leq -19$  and Galactic latitudes  $b > |25^\circ|$ . The LEDA database was also used to identify the faint neighbours in the field of the selected galaxies. The isolation criteria include a  $B$ -band magnitude difference  $> 0.7$  between the primary galaxy and the neighbouring galaxies within a projected distance of 1 Mpc, or  $> 2.2$  magnitudes within 500 kpc. They did not include any redshift information in their isolation criteria. They used the published data from the UK and Palomar Schmidt Sky Survey plates to select all detected dwarf galaxies with absolute magnitudes of  $M_B \leq -14.6$  in the field of the primary galaxies. The sample of dwarfs brighter than  $M_B = -16.8$  or with low surface brightness are incomplete.

*Stocke et al. (2004)* - a sample of early-type galaxies were selected from the Karachentseva (1973) catalogue. Thirteen galaxies were eliminated from the initially selected sample after checking the POSS plates and finding some comparably sized companions missed by Karachentseva (1973). Some of the sample galaxies are too faint and compact to be classified correctly by POSS. So for 80% of the Es and 86% of the S0s galaxies, the morphology and isolation were examined by Stocke et al. using optical imaging taken at Mt. Hopkins 0.6-m telescope and from images included in Adams, Jensen & Stocke (1980). That lead to the elimination of a further seven galaxies. Thus the final sample consists of 62 E and 36 S0 galaxies.

Having decided that some of the previous isolated galaxy samples were not suitable for our purpose, we have defined a new sample.

### 3 SAMPLE SELECTION

Our sample of candidate isolated early-type galaxies was taken from the LEDA. This catalogue contains information on  $\sim 100,000$  galaxies, of which  $\sim 40,000$  have enough information recorded to be of use in this work. From this sample, we selected galaxies which satisfied the following criteria:

- Morphological type  $T \leq -3$ , i.e. early-type.
- Virgo corrected recession velocity  $V \leq 9,000 \text{ km s}^{-1}$ , i.e. within 120 Mpc.
- Apparent magnitude  $B \leq 14.0$ .
- Galaxy not listed as a member of a Lyon Galaxy Group (Garcia 1993).

The restrictions on apparent magnitude and recession velocity were imposed to minimize the effect of incompleteness in the catalogue. The LEDA catalogue is known to be 90% complete at  $B = 14.5$  (Amendola et al. 1997), so our sample should be close to being 100% statistically complete. The selection process produced 330 galaxies which could be considered as potential candidates. These were compared to the rest of the catalogue and accepted as being isolated if they had no neighbours which were within:

- $700 \text{ km s}^{-1}$  in recession velocity,
- 0.67 Mpc in the plane of the sky, and
- 2.0  $B$ -band magnitudes of the isolated galaxy.

These criteria were imposed to ensure that the galaxies did not lie in groups or clusters and that any neighbouring galax-

**Table 1.** The sample of 36 isolated galaxies.

Galaxy	Type	$B_T$ (mag)	Magnitude source	Dist. (Mpc)	Previous samples
NGC 682	E/S0	14.36	LEDA	73	
NGC 821	E	11.33	LEDA	23	SMG03
NGC 1041	E/S0	14.28	LEDA	93	
NGC 1045	E/S0	13.45	LEDA	60	
NGC 1132	E	13.03	LEDA	92	CMZ01
NGC 1162	E	12.88	LEDA	51	SMG03
NGC 2110	E/S0	12.21	LEDA	28	CMZ01
NGC 2128	E/S0	12.66	NED	44	
NGC 2271	E/S0	12.52	LEDA	32	
NGC 2865	E	11.98	LEDA	35	RLR96
NGC 3562	E	12.99	LEDA	93	
NGC 4240	E	13.31	LEDA	26	
NGC 4271	E/S0	13.48	NED	66	
NGC 4555	E	13.05	LEDA	90	
NGC 6172	E	13.75	LEDA	67	CMZ01
NGC 6411	E	12.47	LEDA	53	SMG03
NGC 6653	E	13.02	LEDA	66	SMG03
NGC 6702	E	12.61	LEDA	66	CMZ01
NGC 6776	E	12.51	LEDA	70	
NGC 6799	E	12.98	LEDA	65	RLR96, CMZ01
NGC 6849	E/S0	12.93	LEDA	79	CMZ01
NGC 7330	E	12.66	NED	74	
NGC 7796	E	12.08	LEDA	42	
MCG-01-27-013	E/S0	14.71	LEDA	121	
MCG-01-03-018	E/S0	14.13	LEDA	77	
MCG-02-13-009	E	13.04	LEDA	73	
MCG-03-26-030	E/S0	14.26	LEDA	119	
ESO 107-G004	E	12.55	LEDA	39	
ESO 153-G003	E	13.66	NED	84	
ESO 194-G021	E/S0	13.34	LEDA	41	
ESO 218-G002	E	13.66	LEDA	54	
ESO 318-G021	E	13.24	LEDA	62	RLR96
ESO 462-G015	E	12.46	LEDA	77	
IC 1211	E	13.48	LEDA	78	
UGC 1735	E	13.42	NED	109	
UGC 2328	E	13.11	NED	68	

Notes: Hubble types are from LEDA.  $B_T$  is the total  $B$  magnitude corrected for Galactic extinction from Schlegel et al. (1998). The sources of the  $B$  magnitude are listed in the next column. Distances obtained using the Virgo corrected recession velocities (from LEDA) with  $H_0 = 75 \text{ km s}^{-1} \text{ Mpc}^{-1}$ . Some galaxies were listed in previous samples such as: Reduzzi, Longhetti & Rampazzo (1996, RLR96), Colbert, Mulchaey & Zabludoff (2001, CMZ01) and Smith, Martinez & Graham (2003, SMG03).

**Table 2.** The comparison sample.

Galaxy	Type	$B_T$ (mag)	Magnitude source	Dist. (Mpc)	Environment
IC 4320	S0	13.85	NED	89	Isolated pair
NGC 3528	S0	12.88	LEDA	48	Group
NGC 3557	E	10.79	NED	38	Group
NGC 4697	E	10.02	LEDA	17	Group
NGC 5266	E/S0	11.17	LEDA	38	Group

Notes: Same as Table 1 for the comparison sample. The table includes the environment of each galaxy.

ies were too small and too distant to have any significant effect on the primary galaxy.

To check the results of this process, all galaxies were compared to the NED and the DSS. A NED search in the area within 0.67 Mpc of the galaxy identified galaxies which are not listed in LEDA. We also examined the DSS images for galaxies of similar brightness to the target which are not

listed in either catalogue. This process produced 36 candidate isolated early-type galaxies. Basic data for this sample are listed in Table 1. In this paper we present imaging for 10 of these galaxies. We have also included IC 4320 which is a part of an interacting isolated galaxy pair (with the spiral ESO509-G100). They have a  $B$ -magnitude difference of 0.88 and recession velocity difference of  $260 \text{ km s}^{-1}$ . The

projected distance between them is 8.2 arcmin or 212 kpc (Soares et al. 1995). We also include imaging of a few galaxy groups to act as a comparison to our isolated galaxies. These are the NGC 3557 (LGG 229), NGC 4697 (LGG 314) and NGC 5266 (LGG 356) groups. In our comparison group sample, we also have included NGC 3528. Although it is not in the Garcia (1993) group catalogue, it has a luminous late-type galaxy (NGC 3529) at a projected distance of 5 arcmin or 70 kpc with  $B$ -band magnitude difference of 1 and recession velocity difference of  $77 \text{ km s}^{-1}$ . There is also a galaxy group (USGC S160) located at a projected distance of 14.8 arcmin or 207 kpc from NGC 3528, with a recession velocity difference of 30 km/s. In addition, there are many intermediate luminosity galaxies in the field of NGC 3528 with no published magnitude and/or velocity. The basic data for our comparison sample are summarized in Table 2.

#### 4 OBSERVATIONS AND DATA REDUCTION

For all galaxies in tables 2 and 3,  $B$  and  $R$ -band images were obtained using the Wide Field Imager (WFI) on the 3.9-m Anglo-Australian Telescope (AAT) on 2002 February 17th-19th. WFI is an 8 CCD imaging mosaic, of  $2048 \times 4096$  pixels thinned back-illuminated CCDs with a pixel scale of  $0.229'' \text{ pix}^{-1}$  giving a field-of-view of  $30.6 \times 30.6$  sq. arcmins. Over the three nights there was some partial cloud and typical seeing conditions of about  $2.0''$  in  $B$  and  $1.5''$  in  $R$ . The exposure times for the galaxies and the number of observations are listed in Table 3. In addition to the galaxies, several standard star fields from Landolt (1992) were obtained. These consisted of 10 sec exposures for both  $B$  and  $R$ -bands.

All galaxy and standard star images were reduced in an identical manner using IRAF tasks. Six of the WFI CCD's have one or two bad columns which were corrected by interpolating the pixel values on both sides of the bad column. Data reduction included subtraction of the overscan regions. These regions were then trimmed before correcting the frames by master bias subtraction, dark frame subtraction and flat fielding using combined dome flats. The final images are flat to  $\leq 2\%$ . We multiplicatively corrected for the different gains between CCDs using measurements of the mean sky level in each CCD, relative to the 'best' CCD (i.e. CCD6 which is cosmetically the cleanest).

After determining an optimal aperture size of 10 pixels ( $\sim 2.3''$ ), based on a curve-of-growth type analysis, raw magnitudes of between 7 and 25 stars were obtained for each filter using the IRAF task QPHOT. The zero-point for each filter was determined by a simple linear fit to the stellar raw magnitude versus their colours published by Landolt (1992) and corrected for airmass. The atmospheric extinction coefficients used were  $k_B = 0.22$  and  $k_R = 0.08$  mag/airmass. The final photometric zero-points are  $Z_B = 25.19 \pm 0.06$  and  $Z_R = 25.93 \pm 0.04$ .

**Table 3.** Observational data of the combined sample.

Galaxy	$A_B$ (mag)	$A_R$ (mag)	Exp. Time
NGC 1045	0.18	0.11	( $B$ ) $1 \times 240$ ( $R$ ) $1 \times 120$
NGC 1132	0.27	0.17	( $B$ ) $1 \times 240$ ( $R$ ) $1 \times 120$
NGC 2110	1.62	1.00	( $B$ ) $1 \times 240$ ( $R$ ) $1 \times 120$
NGC 2865	0.36	0.22	( $B$ ) $1 \times 240$ ( $R$ ) $1 \times 120$
NGC 4240	0.23	0.15	( $B$ ) $1 \times 240$ ( $R$ ) $1 \times 120$
NGC 6172	0.51	0.31	( $B$ ) $1 \times 240$ ( $R$ ) $1 \times 120$
MCG-01-27-013	0.19	0.12	( $B$ ) $2 \times 240$ ( $R$ ) $2 \times 120$
MCG-03-26-030	0.22	0.14	( $B$ ) $1 \times 240$ ( $R$ ) $1 \times 120$
ESO218-G002	0.75	0.46	( $B$ ) $2 \times 120$ ( $R$ ) $2 \times 60$
ESO318-G021	0.35	0.22	( $B$ ) $1 \times 120$ ( $R$ ) $1 \times 60$
IC 4320	0.26	0.16	( $B$ ) $1 \times 240$ ( $R$ ) $1 \times 120$
NGC 3528	0.17	0.11	( $B$ ) $1 \times 240$ ( $R$ ) $1 \times 120$
NGC 3557	0.43	0.26	( $B$ ) $1 \times 60$ , $3 \times 600$ ( $R$ ) $1 \times 60$ , $3 \times 420$
NGC 4697	0.13	0.08	( $B$ ) $1 \times 60$ , $3 \times 600$ ( $R$ ) $1 \times 60$ , $3 \times 420$
NGC 5266	0.38	0.24	( $B$ ) $2 \times 240$ ( $R$ ) $2 \times 120$

Notes: The Galactic extinctions  $A_B$  and  $A_R$  are from Schlegel et al. (1998). The table has been divided into three sections based on environment.

#### 5 MEASURING PHOTOMETRIC PARAMETERS

##### 5.1 Magnitudes and colours

The QPHOT task in IRAF was used to obtain total magnitudes for the primary galaxies in our sample. The sky was generally computed in an annulus of radius 1000 pixels and width of 50 pixels. Total magnitudes were derived by fitting a curve-of-growth to galaxy aperture magnitudes from  $3 \times$  the seeing radius to large radii. Finally, the total magnitudes  $B$  and  $R$  were corrected for Galactic extinction using values from Schlegel, Finkbeiner & Davis (1998) as given in Table 3.

For ESO318-G021 and NGC 4240, the  $B$  frame is dominated by the light from a close bright star which prevented us measuring total  $B$  magnitudes. Considering the typical colour for galaxies in the present sample and the  $B$  magnitude quoted by LEDA, then our measured  $R$  magnitude for both of these two galaxies seems reasonable. A mean total ( $B-R$ ) colour of  $1.46 \pm 0.12$  was obtained for the 13 remaining galaxies. Our measured total  $B$  and  $R$  magnitudes, corrected for Galactic extinction, are given in Table 4. Fig. 1

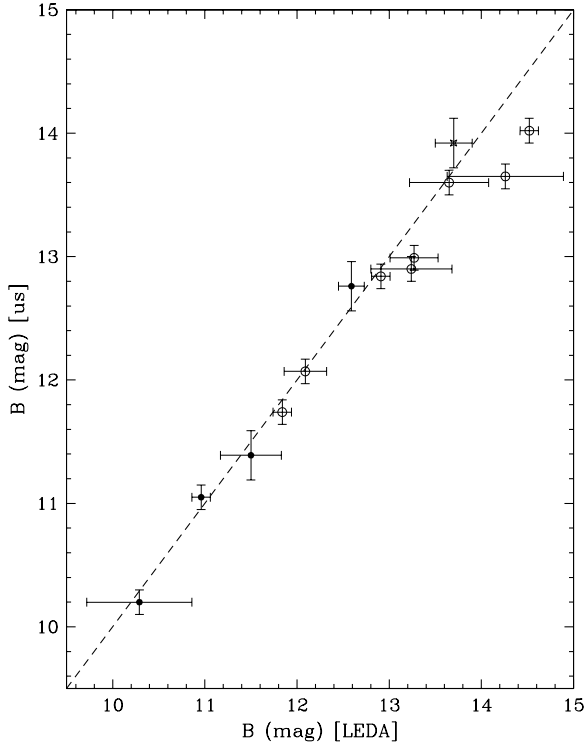


**Figure 1.** Comparison between our measured  $B$  magnitudes and the published values in LEDA. Filled and open circles represent group and isolated galaxies respectively, while the star is the primary galaxy of an isolated pair (IC 4320). Our measurements show good consistency with values from LEDA.

shows the good agreement between our  $B$  magnitudes compared to the published values from LEDA.

## 5.2 Modelling and surface brightness profile fitting

Visual inspection of our CCD images of the 15 galaxies in our sample confirms their early-type morphology as published in LEDA. The ISOPHOTE package in IRAF was used to fit a smooth elliptical model to the galaxy image (e.g. Forbes & Thompson 1992). In this package the isophotes are fit using an iterative method described by Jedrzejewski (1987). Before modelling the galaxy, the sky value was determined and subtracted. The program starts at a small radius and increases to large radii in a geometrical progression. The galaxy centre, position angle and ellipticity were allowed to vary.

Since our sample consists of early-type galaxies with absolute magnitudes in the range  $-19.2 > M_B > -22.1$  their surface brightness profiles can be well fit by a de Vaucouleurs  $R^{1/4}$  law (Prugniel & Simien 1997). By fitting the surface brightness profiles we derived the effective radii ( $R_e$ ) and mean surface brightnesses ( $\langle \mu_e \rangle$ ) within  $R_e$ . To avoid resolution effects, the fitting was applied from a radius of about  $3 \times$  the seeing to large radii. In the case of NGC 5266 there is a strong dust ring around the galaxy (see also Goudfrooij et al. 1994a). This prevented us from deriving a reliable surface

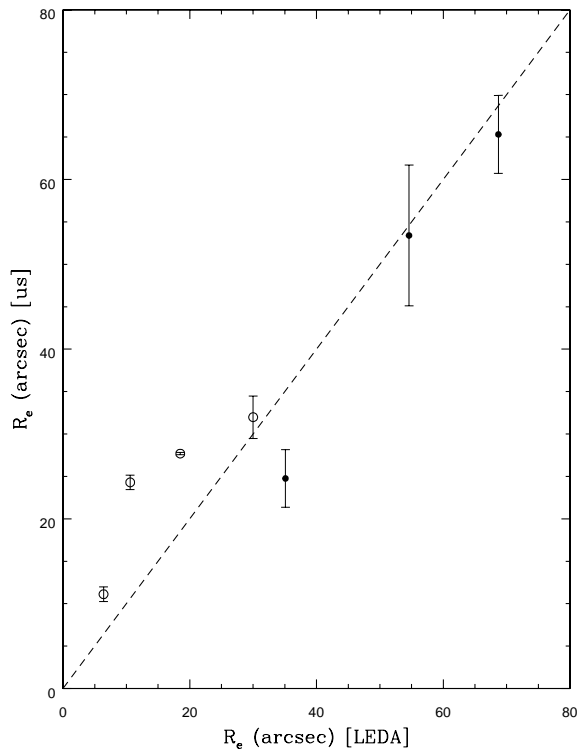


**Figure 2.** Comparison between the effective radius  $R_e$  measured from our  $R$ -band images and the published values in LEDA. Error bars represent the variation during the fitting. Generally, the agreement is good. Symbols as in Fig. 1.

brightness profile and parameters in the  $B$ -band. However for the  $R$ -band, only a small region of the profile was affected. This was masked and excluded from the fit. We were also unable to measure reliable profiles in the  $B$  and  $R$ -bands for NGC 4240 and the  $B$ -band for ESO318-G021, due to the bright nearby stars.

Using the ellipticity ( $\epsilon$ ) and the effective semi-major axis ( $a_e$ ) from the galaxy model, the effective radius  $R_e$  was calculated, i.e.  $R_e = a_e \sqrt{1 - \epsilon}$ . The values of  $R_e$ , and its error estimate based on the variation during the fitting procedure, are given in Table 4. There is generally good agreement between the  $B$  and  $R$ -band effective radii determinations. Fig. 2 shows that our measured values of  $R_e$  from the  $R$ -band images and the corresponding values from LEDA, for four isolated and three group galaxies for which data are available, are comparable.

The  $(B-R)_e$  colours at  $R_e$  (Table 4) are obtained from the models using the difference between the  $B$  and  $R$ -band surface brightness profiles. The exact radius used does not strongly affect the  $(B-R)_e$  colour because of the shallow slope in the colour gradient. Fig. 3 shows good agreement between our derived colours and those given in LEDA, when available.

The mean surface brightness within  $R_e$  in each filter is calculated as:  $\langle \mu_e \rangle = 2.5 \log[\pi R_e^2] + m(R_e)$ , where  $m(R_e)$  is the enclosed magnitude within  $R_e$  estimated from the model. Table 5 lists the mean surface brightnesses within the effective radius in the  $B$  and  $R$ -bands.

**Table 4.** Measured photometric and size parameters.

Galaxy	$B$ (mag)	$\pm$	$R$ (mag)	$\pm$	$(B-R)_e$ (mag)	$\pm$	$R_e(B)$ (arcsec)	$\pm$	$R_e(R)$ (arcsec)	$\pm$
NGC 1045	13.0	0.1	11.4	0.1	1.63	0.14	15.7	4.2	16.7	1.6
NGC 1132	12.9	0.1	11.6	0.1	1.70	0.14	29.8	3.6	32.0	3.5
NGC 2110	11.7	0.1	10.3	0.1	1.47	0.14	28.3	1.4	24.3	1.2
NGC 2865	12.1	0.1	10.8	0.1	1.26	0.14	28.3	0.8	27.7	0.2
NGC 4240	-	-	11.3	0.1	-	-	-	-	-	-
NGC 6172	13.6	0.1	12.3	0.1	1.44	0.14	12.4	1.9	11.1	1.2
MCG-01-27-013	14.0	0.1	12.5	0.1	1.58	0.14	16.1	2.1	13.8	0.9
MCG-03-26-030	13.7	0.1	12.1	0.1	1.63	0.14	14.3	0.6	15.6	2.5
ESO218-G002	12.8	0.1	11.4	0.1	1.58	0.14	22.0	6.6	20.1	5.0
ESO318-G021	-	-	12.1	0.1	-	-	-	-	21.7	3.2
IC 4320	13.9	0.2	12.3	0.1	1.59	0.22	27.6	9.5	22.4	4.5
NGC 3528	12.8	0.2	11.2	0.1	1.63	0.22	43.2	15.	45.6	0.9
NGC 3557	11.1	0.1	9.6	0.1	1.57	0.14	29.7	4.2	24.8	4.8
NGC 4697	10.2	0.1	8.8	0.1	1.46	0.14	86.9	9.9	65.3	6.5
NGC 5266	11.4	0.2	9.9	0.1	1.31	0.22	-	-	53.4	11.7

Notes: The table lists total magnitudes, colour at the effective radius and the effective radius itself.

**Table 5.** Derived parameters.

Galaxy	$M_B$ (mag)	$\pm$	$M_R$ (mag)	$\pm$	$\langle \mu_e \rangle_B$ (mag/sq.”)	$\pm$	$\langle \mu_e \rangle_R$ (mag/sq.”)	$\pm$	$\log(R_e)_B$ (kpc)	$\pm$	$\log(R_e)_R$ (kpc)	$\pm$
NGC 1045	-20.9	0.1	-22.5	0.1	20.8	0.1	19.4	0.1	0.66	0.10	0.69	0.04
NGC 1132	-21.4	0.1	-23.2	0.1	22.5	0.1	21.0	0.1	1.12	0.05	1.14	0.06
NGC 2110	-20.5	0.1	-21.9	0.1	20.7	0.1	19.0	0.1	0.59	0.02	0.52	0.02
NGC 2865	-20.6	0.1	-21.9	0.1	20.8	0.1	19.5	0.1	0.68	0.01	0.67	0.01
NGC 4240	-	-	-20.8	0.1	-	-	-	-	-	-	-	-
NGC 6172	-20.5	0.1	-21.8	0.1	20.8	0.1	19.1	0.1	0.61	0.06	0.56	0.06
MCG-01-27-013	-21.4	0.1	-22.9	0.1	22.0	0.1	20.1	0.1	0.97	0.05	0.91	0.03
MCG-03-26-030	-21.7	0.1	-23.3	0.1	21.4	0.1	19.9	0.1	0.92	0.02	0.95	0.07
ESO218-G002	-20.9	0.1	-22.3	0.1	21.5	0.1	19.8	0.1	0.76	0.11	0.72	0.10
ESO318-G021	-	-	-21.9	0.1	-	-	20.6	0.2	-	-	0.81	0.06
IC 4320	-20.9	0.2	-22.5	0.1	22.7	0.2	20.8	0.1	1.08	0.13	0.99	0.08
NGC 3528	-20.6	0.2	-22.2	0.1	22.4	0.2	20.9	0.1	1.00	0.13	1.03	0.01
NGC 3557	-21.8	0.1	-23.3	0.1	20.5	0.1	18.6	0.1	0.74	0.06	0.66	0.08
NGC 4697	-21.0	0.1	-22.4	0.1	21.4	0.1	19.5	0.1	0.86	0.05	0.73	0.04
NGC 5266	-21.5	0.2	-23.0	0.1	-	-	20.1	0.1	-	-	0.99	0.09

Notes: The table lists absolute magnitudes, mean surface brightness within the effective radius and the effective radius in kpc.

### 5.3 Isophotal shape parameters

The modelling process fits elliptical isophotes to the galaxy images and measures their isophotal shape parameters. Figures 4-7 show the radial profile of these parameters in the  $R$ -band for the fourteen galaxies which could be successfully modelled (i.e. excluding NGC 4240). These isophotal shape parameters help define the morphology of the galaxy. For example, the 4<sup>th</sup>-order cosine term of the Fourier series is a useful parameter to express the deviation from a perfect ellipse due to the presence of additional light. An excess of light along the major and/or minor axes (called *disky*) is indicated by positive values, while negative values indicate excess light at 45° with respect to these axes (called *boxy*).

To quantify the 4<sup>th</sup>-order cosine parameter we applied a technique similar to that of Bender et al. (1989). When

the fourth-order cosine profile shows a peak or a minimum, then the maximum amplitude is taken, while in case of a monotonically changing profile we use the value at  $R_e$ . In the case of more complicated profiles indicated by a radial change from *disky* to *boxy* (or vice versa), such galaxies are classified as *irregular* (irr). Table 6 lists the 4<sup>th</sup>-order cosine values normalised to the semi-major axis. It also lists the difference between the maximum and minimum values of the position angle for each galaxy after avoiding the inner, seeing-affected regions.

### 5.4 Residual images

Another way to study the morphology or fine structure of an elliptical galaxy is by examining the residual image, i.e. the original image minus the galaxy model. Using the

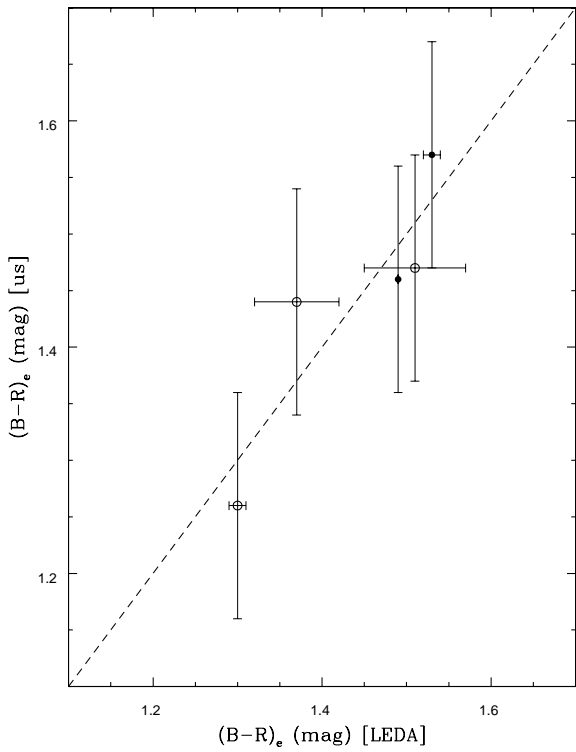


**Figure 3.** Comparison between our measured colour at the effective radius  $(B-R)_e$  and the published values in LEDA. Generally, the agreement is very good. Symbols as in Fig. 1.

**Figure 4.** The  $R$ -band (open circles) surface brightness, ellipticity, position angle and  $4^{th}$ -order cosine profiles. The upper panel for each galaxy shows also the  $B$ -band surface brightness (solid circles). The name of each galaxy is written above each set of four panels. [See fig4to7.tar]

**Figure 5.** Same as Fig. 4. [See fig4to7.tar]

**Figure 6.** Same as Fig. 4. [See fig4to7.tar]

**Figure 7.** Same as Fig. 4. [See fig4to7.tar]

**Figure 8.** Residual images of galaxies (with filters given in brackets): NGC 1045( $R$ ), NGC 1132( $R$ ), NGC 2110( $R$ ), NGC 2865( $R$ ), NGC 6172( $R$ ), MCG-01-27-013( $R$ ), MCG-03-26-030( $R$ ), ESO218-G002( $R$ ) and ESO318-G021( $R$ ) (left to right, top to bottom). Dust regions can be seen as bright features and extra light as dark features. All images have the same size of  $188 \times 155$  sq. arcsec and oriented as North up and East to the left. [See fig8and9.tar]

**Figure 9.** Residual images of IC 4320( $B$ ), NGC 3528( $B$ ), NGC 3557( $R$ ), NGC 4697( $R$ ) and NGC 5266( $B$ ) (left to right, top to bottom). Orientations and sizes as in Fig. 8. [See fig8and9.tar]

**Figure 10.** The size-magnitude relation for detected galaxies in the field of (a) the isolated galaxy ESO218-G002 and (b) the NGC 3528 group. The SExtractor parameters A\_IMAG and MAG\_BEST were used as a measure of size and magnitude respectively. The vertical dotted line represents our 100% completeness limit of  $R = 18.75$ . For ESO218-G002 the brightest galaxy in the field is  $\sim 4$  mags fainter and  $\sim 1/3$  the size of ESO218-G002 itself. [See fig10.gif]

**Table 6.** Isophotal shape parameters.

Galaxy	$4^{th}$ cosine %	$\Delta PA$ ( $^{\circ}$ )
NGC 1045	-3.5	0
NGC 1132	-1.5	10
NGC 2110	irr	12
NGC 2865	+1.5	14
NGC 6172	irr	25
MCG-01-27-013	+1.0	14
MCG-03-26-030	+2.0	2
ESO218-G002	0	70
ESO318-G021	0	8
IC 4320	irr	30
NGC 3528	+3.2	10
NGC 3557	0	0
NGC 4697	+2.0	2
NGC 5266	irr	8

Notes: The percentage  $4^{th}$  cosine term of the Fourier series is normalised to the semi-major axis. The difference between the maximum and minimum position angles are quoted for radii greater than 10 arcsec.

BMODEL task in IRAF we created a 2D model of the galaxy. This model represents the smooth elliptical structure of each galaxy. Subtracting this model from the original image gives the residual image which better reveals any fine structure (e.g. dust, shells, tidal tails, boxy or disk-like structure, etc.) hidden underneath the dominant elliptical light of the galaxy. Figures 8 and 9 display the residual images of the sample galaxies (excluding NGC 4240).

## 6 FAINT GALAXY DETECTION

As our images cover a field-of-view of hundreds of square kiloparsecs surrounding each galaxy, they allow us to probe the distribution of galaxies in their fields. With the strict isolation criteria used to select galaxies in this study, the area surrounding the primary galaxy will contain no bright galaxies (within  $\sim 2$  mags) but may still contain many faint ones. The detection of these faint galaxies was performed using SExtractor version 2.3 (Bertin & Arnouts 1996). From the deeper  $R$ -band images, all objects with more than 10 connected pixels that are  $3\sigma$  above the sky background were identified. To estimate the background level of the images, as well as the RMS noise in the background, we set the mesh size to 200 pixels. This value of the mesh size was found to be suitable for extended object detection. The image was then smoothed with a median filter of  $10 \times 10$  pixels to remove any fluctuations resulting from bright or extended objects. The photometric parameter MAG\_BEST was used

as a measure of the total magnitude. A comparison between MAG\_BEST magnitudes and the corresponding total magnitudes measured with the IRAF task QPHOT showed good agreement.

For star-galaxy separation, we used the CLASS\_STAR parameter (ICLASS) defined by SExtractor. Running SExtractor on the 60 sec and the combined (1320 sec)  $R$  band mosaic frames of the NGC 3557 group, we obtained two sets of detected bright objects, i.e. stars and galaxies with ICLASS parameters of 1 and 0 respectively. For faint objects ( $R \geq 18$ ), ICLASS values ranged from 0 to 1. Visual inspection of the 60 sec and combined images revealed that an ICLASS value of 0.09 provided a good separation between resolved galaxies and stellar-like objects. Thus objects with  $\text{ICLASS} > 0.09$  were removed from all of our object lists. After displaying all the remaining detections, we removed the small number of obvious mis-identifications (e.g. bad columns, diffraction spikes, halos of bright stars, etc.). Finally, for the isolated galaxies, we searched the NED database and excluded any of the detected faint galaxies that have a published velocity difference of greater than 700 km  $\text{s}^{-1}$  from the parent galaxy. This resulted in only a handful of galaxies being removed for the isolated galaxy sample.

In order to estimate our magnitude completeness limits, we compared the 60 and 420 sec to the combined (1320 sec) frame of the NGC 3557 group. This allows us to estimate our completeness as a function of exposure time. For example, a typical 120 sec exposure has an estimated 100% completeness limit of  $R = 18.75$ . Except for ESO318-G021, all other galaxies have a total exposure time of at least 120 sec (Table 3).

Using the SExtractor parameter A\_IMAG as a measure of galaxy size, Fig. 10 shows the size-magnitude distribution after our selection criteria and visual inspection are applied. The figure shows the isolated galaxy ESO218-G002 and the NGC 3528 group which are at almost same distance and have the same exposure time of 120 sec. The vertical line indicates our 100% completeness limit of  $R = 18.75$ . For ESO218-G002 the brightest galaxy in the field is  $\sim 4$  mag fainter and  $\sim 1/3$  the size of ESO218-G002 itself. As a result of the SExtractor process, we have a list of apparent magnitudes, projected distances in kpc from the primary galaxy and angular sizes of galaxies in the field of the primary galaxy.

## 7 RESULTS AND DISCUSSION

In this section we first discuss our results about the primary galaxy sample and then the results related to the detected galaxies in their fields.

### 7.1 Colours of isolated galaxies

Prugniel & Heraudeau (1998), using a sample of 5,169 galaxies, measured the colour for 80 galaxies to be  $(B-R)_e = 1.52 \pm 0.2$  and for ellipticals  $(B-R)_e = 1.57 \pm 0.2$ . These values are consistent with the measured effective colours of our sample (see Table 4) which have a mean of  $(B-R)_e = 1.54 \pm 0.14$ . We note that NGC 2865 is quite blue with  $(B-R)_e = 1.26 \pm 0.14$ .

The CMR of ellipticals was discovered by Baum (1959)

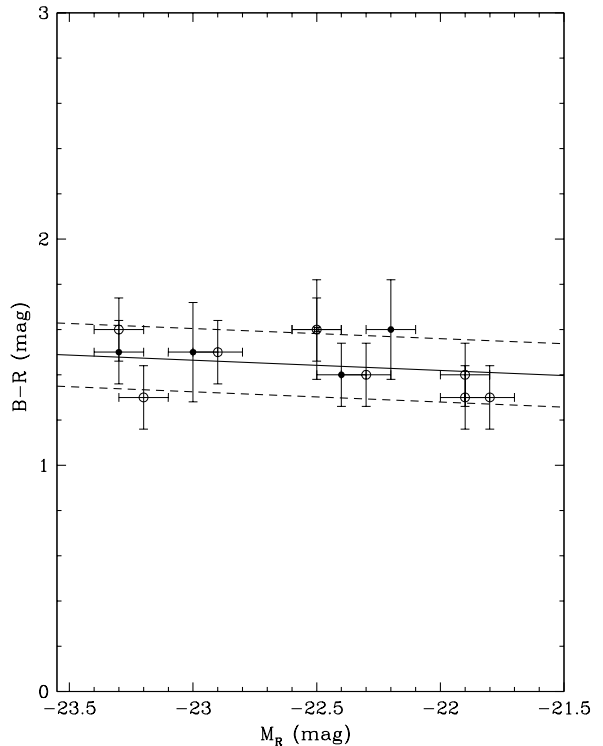


**Figure 11.** Colour-magnitude relation for the sample galaxies. The solid line (Gladders et al. 1998) represents the CMR of elliptical galaxies in the Coma cluster, while the dashed line indicates the mean error in the colour measurements for our sample galaxies. The isolated galaxies are consistent with the Coma cluster CMR. Symbols as in Fig. 1.

when he studied the stellar content for a sample of elliptical galaxies and globular clusters. He found more luminous ellipticals to be redder. Further studies of cluster ellipticals have shown that the CMR is a linear relation with a small intrinsic scatter (e.g. Bower, Lucey & Ellis 1992). A comparison of the observed slope and scatter of the CMR with that expected from theoretical models, has been used by many authors to constrain the formation epoch of the bulk of stars in early-type cluster galaxies to be at  $z > 2$  (e.g. Bower et al. 1992; Stanford, Eisenhardt & Dickinson 1995; Ellis et al. 1997; Stanford et al. 1998; Bower, Kodama & Terlevich 1998; Bernardi et al. 2003). The constant slope out to high redshifts means that the CMR is generally interpreted as a relation of mass with metallicity (Kodama 2001); while the scatter, although small, is due to ongoing star formation.

In Fig. 11, we show that our isolated galaxies are reasonably well matched by the  $B-R$  CMR for the Coma cluster derived by Gladders et al. (1998). We used total  $B-R$  colours as they are the closest match to the aperture magnitudes of Gladders et al. Fixing the slope to the Gladders et al. value, we measure a scatter of  $\sim 0.12$  mag for the isolated galaxies, which is similar to our photometric errors. Thus the scatter is largely intrinsic and consistent with the estimated low scatter found for early-type galaxies in clusters (Bower et al. 1992; Stanford et al. 1998).

## 7.2 Fine structure

Many studies have found that elliptical galaxies have light distributions which deviate from perfect ellipticity (Lauer 1985; Bender, Döbereiner & Möllenhoff 1988; Franx, Illingworth & Heckman 1989; Peletier et al. 1990; Bender & Möllenhoff 1987; Forbes & Thomson 1992; Goudfrooij et al. 1994b). These deviations can be due to dust lanes or extra-light structures. Such morphological features could be a result of the tidal disruption of a small companion (Binney & Petrou 1985; Nieto & Bender 1989) or a major merger (Schweizer et al. 1990). In a detailed study of boxiness in massive ellipticals by Nieto & Bender (1989) and Bender et al. (1989), the isophotal shape showed little or no correlation with the classic photometric parameters such as luminosity, effective radius or ellipticity. However, galaxies which were radio-loud and/or surrounded by gaseous X-ray halos generally had boxy or irregular isophotes. Bender et al. also found that galaxies with boxy or irregular isophotes seem to have higher mass-to-light ratios ( $\sim 11.5 \pm 0.9 M_\odot/L_\odot$ ) than disk galaxies ( $\sim 6.4 \pm 0.6 M_\odot/L_\odot$ ).

Our isolated galaxy sample reveals a range of fine structure from plumes and shells to dust lanes, and some galaxies with no detectable fine structure. Good examples of boxy and disk isophotes can be seen in NGC 1045 and NGC 4697 respectively. Shells (in the case of NGC 2865) and dust lanes appear to affect the 4<sup>th</sup>-order cosine profile of many galaxies. The presence of internal structures such as dust, shells, disk or boxy structure could be the result of a past merger (e.g. Forbes 1991; Barnes & Hernquist 1992; Balcells 1997; Merluzzi 1998; Khochfar & Burkert 2003). Including plumes, shells and dust, 4 out of 10 isolated galaxies reveal signs of a past merger or accretion event. The isolated galaxies ESO218-G002 and ESO318-G021 are good examples of no obvious fine structure. From the radial profiles (Table 6) and the residual images of each galaxy (Figures 8 and 9), the following features were revealed:

**NGC 1045:** The isophotes are strongly boxy out to a semi-major axis radius of 35''. Probable dust along the semi-major and semi-minor axes. There is extensive extra tidal light surrounding the galaxy. This galaxy is a probable merger remnant.

**NGC 1132:** No obvious features. Classified as a fossil galaxy by Mulchaey & Zabludoff (1999).

**NGC 2110:** Probable dust traces in the central region. Contains a seyfert nucleus (Pfefferkorn, Boller & Rafanelli 2001).

**NGC 2865:** Extra tidal light (shells) to the east and north east. Probable dust in the inner region. This galaxy is a probable merger remnant (see also Hau, Carter & Balcells 1999).

**NGC 4240:** Nearby bright star. No obvious features.

**NGC 6172:** No obvious features.

**MCG-01-27-013:** Weak disk structure at radius  $\sim 15''$ .

**MCG-03-26-030:** Disky beyond 10''. Probable dust.

**ESO218-G002:** No obvious features. Large position angle twist seen.

**ESO318-G021:** Nearby bright star. No obvious features.

**IC 4320:** Strong dust lane within central 20''. Probably a merger remnant.

**NGC 3528:** Strong dust lane extending from the north east to south west. Probably a merger remnant.

**NGC 3557:** No obvious features.

**NGC 4697:** Strong disk structure extending to  $\sim 40''$ .

**NGC 5266:** Dust ring around galaxy. Probably a merger remnant.

Thus, some isolated galaxies reveal signatures of a past interaction/merger while others look featureless and undisturbed. Zepf & Whitmore (1993) found 50% of their Hickson compact group elliptical sample to have irregular isophotes compared to  $\lesssim 21\%$  in loose groups and clusters. Our sample, although small, does not show a predominance of irregular isophotes, and appears similar to the distribution of isophotal shapes for loose groups and cluster ellipticals suggesting a similar frequency of mergers and interactions. Our isolated galaxy sample includes 44% (4/9) with dust and 11% (one galaxy; NGC 1045) with tidal tails which is a higher percentage than that found by Reduzzi, Longhetti & Rampazzo (1996) who quote a percentages of 24.6% and 3.3% respectively. Colbert et al. (2001) detected 75% of early-type galaxies in low-density environments to have dust. The galaxies with shells in our sample show a similar percentage of 11% (one galaxy; NGC 2865) compared to 16.4% in the sample of Reduzzi et al. (1996). Overall, our isolated galaxies show evidence of past mergers (shells, dust, tidal tails, etc) in 44% of the total sample which is similar to the corresponding percentage in Reduzzi et al. (1996).

## 7.3 Kormendy relation

Kormendy (1977) found that the effective radius ( $R_e$ ) of elliptical galaxies is correlated with the surface brightness at  $R_e$  ( $\mu_e$ ). Based on a larger sample, Hamabe & Kormendy (1987) found this correlation in the  $V$ -band to be  $\mu_e = 2.94 \log(R_e) + 19.48$ .

Many studies have used this relation to investigate galaxy evolution with environment and look-back time. For example, Hoessel, Oegerle & Schneider (1987) studied 372 elliptical galaxies in 97 nearby ( $z < 0.1$ ) Abell clusters and found that the brightest cluster galaxies to have a  $R_e$ - $\mu_e$  relation very similar to that in Hamabe & Kormendy (1987). However they also found that the less luminous ellipticals in the cluster cores had a steeper relation with a slope of 4.56, in the sense that at a given surface brightness these galaxies have smaller effective sizes. The distinction of the two different luminosity groups became more obvious in a later study by Capaccioli, Caon & D'Onofrio (1992) with a larger sample of Virgo cluster galaxies and other data collected from the literature. They confirmed that, unlike the low luminosity galaxies, the brightest cluster galaxies fit perfectly on the Hamabe & Kormendy relation. In a recent study by Khosroshahi et al. (2004), the Kormendy relation was explored for early-type galaxies in groups that have a range of X-ray luminosities. They found that group early-type galaxies show a similar relation to those in clusters. Up to redshifts of  $z \sim 1.5$ , elliptical galaxies in clusters show a similar relation to cluster galaxies in the local universe, with no significant change in the slope or scatter (Ziegler et al. 1999; Waddington et al. 2002; La Barbera et al. 2003).

The distribution of our isolated galaxies in the  $\log(R_e)$ - $<\mu_e>$  plane, where  $<\mu_e>$  is the mean surface brightness within  $R_e$ , is shown in Fig. 12. Using the relation between  $\mu_e$  and  $<\mu_e>$  (Graham & Colless 1997) and assuming typical colours of  $B-V = 0.8$  and  $B-R = 1.5$ , we reproduce the

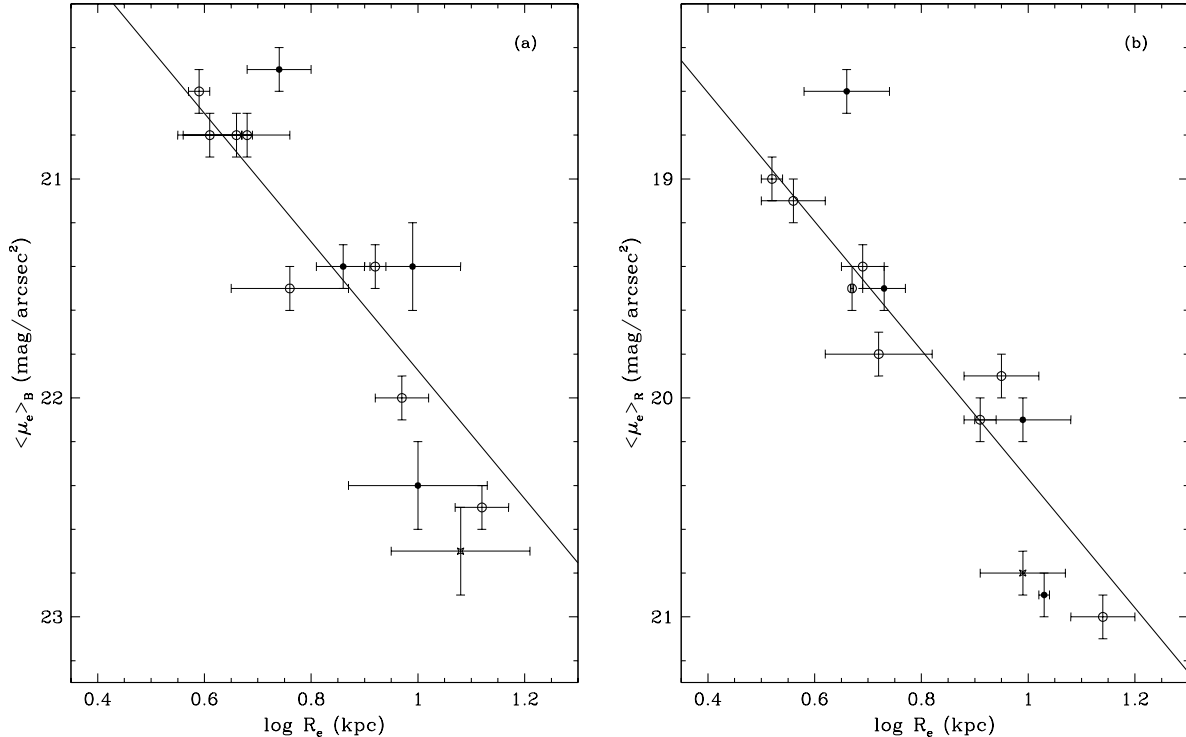


**Figure 12.** The Kormendy relation between the mean surface brightness within the effective radius and effective radius in the  $B$  and  $R$ -bands. The solid line represents the original Hamabe & Kormendy (1987) relation. The zero-point of the original relation has been shifted from  $V$  to the  $B$  and  $R$ -bands assuming typical colours of  $B-V = 0.8$  and  $B-R = 1.5$ . Our isolated galaxies are generally consistent with the Hamabe & Kormendy relation for luminous galaxies. Symbols as in Fig. 1.

Hamabe & Kormendy relation in the  $B$  and  $R$ -bands in Fig. 12. Our isolated galaxies are generally consistent with the Hamabe & Kormendy relation for luminous galaxies.

#### 7.4 The gravitational effect of faint companions

Here, we have assumed that all detected faint galaxies in the field surrounding a galaxy lie at the same redshift as the primary galaxy (in reality many will be background objects) and have calculated their luminosity  $L_R$  in the  $R$ -band. For an assumed mass-to-light ratio of  $M/L_R = 10 M_\odot/L_\odot$ , we estimated the mass  $M$  of each faint galaxy. For all faint galaxies in the field of a primary galaxy, we have calculated the dynamical friction timescale using equation 7-27 in Binney & Tremaine (1987). We assumed a velocity dispersion of  $\sigma = 250 \text{ km s}^{-1}$  for the galaxies in the field of the isolated galaxy. As galaxies with dynamical friction times that are significantly less than the Hubble time should have merged with the primary galaxy, and hence not be visible, their existence suggests that they may actually lie in the foreground or background. In the case of the four groups, we used the published velocities in NED to remove the non-group members.

The gravitational effect applied on the primary galaxy by each of the faint galaxies in its field is proportional to  $M/R^2$ , where  $R$  is the projected distance of the faint galaxy from the primary galaxy. Except for the faint dwarfs with short dynamical friction times and non-group mem-

bers, we calculate the parameter  $M/R^2$  for all detected galaxies in the field of the 10 isolated and 4 group galaxies. Fig. 13 shows the number distribution of the  $M/R^2$  values for the isolated and the group galaxies. In the case of groups, the distribution has been scaled up by a factor of  $2.5 \times$ . Comparing the fields of the isolated and group galaxies we notice the absence of galaxies with  $M/R^2$  greater than  $\sim 4 \times 10^6 M_\odot/\text{kpc}^2$  for isolated galaxies. This is a further indication that our isolated galaxies are indeed gravitationally isolated.

#### 7.5 Luminosity function

The Luminosity Function (LF) represents the number distribution of galaxies in a given magnitude interval. Traditionally, this distribution is fit with a function of the form  $\phi(L) = (\phi^*/L^*) (L/L^*)^\alpha e^{(L/L^*)}$  with  $L^*$  and  $\alpha$  representing a characteristic bright magnitude and the slope of the faint end respectively (Schechter 1976). The importance of the LF lies in its strong correlation with the mass function of the galaxy distribution, which is one of the observable tests of any theoretical cosmological model. It may also provide clues to the evolutionary history of galaxies. There have been several studies of the LF for high-density cluster environments (Trentham & Hodgkin 2002; Mobasher et al. 2003; Christlein & Zabludoff 2003) and lower density regions such as groups (Zabludoff & Mulchaey

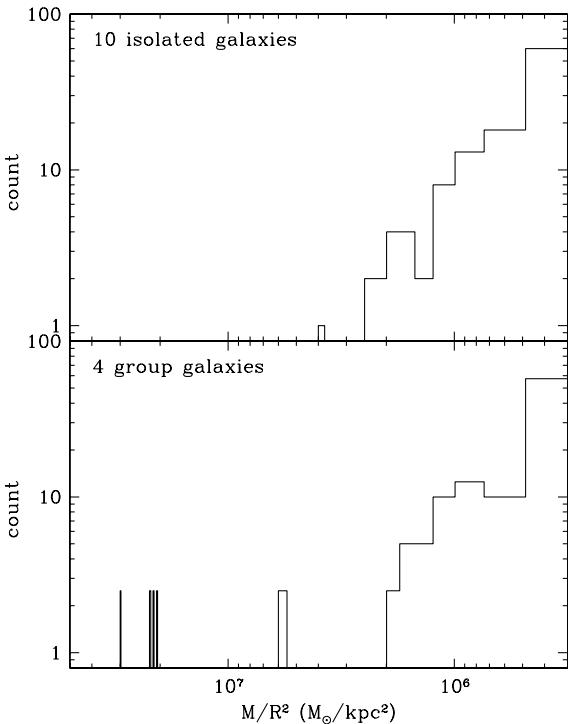


**Figure 13.** Number distribution of  $M/R^2$  values for the 10 isolated and 4 group galaxies. The group galaxies have been scaled up in number by a factor of  $2.5 \times$  to match the isolated galaxy sample.  $M$  is the mass of the detected galaxy in solar masses and  $R$  is the projected distance of the galaxy from the primary galaxy in kpc. The value  $M/R^2$  represents the gravitational force applied on the primary galaxy by the faint galaxies in its local environment (assuming they lie at the same redshift). Unlike the group galaxies, the isolated galaxies are not influenced by the gravitational effects of faint neighbours with  $M/R^2 \gtrsim 4 \times 10^6 M_\odot/\text{kpc}^2$ .

2000; Flint, Bolte & Oliveira 2003) and the field (Blanton et al. 2001; Blanton et al. 2003; Drory et al. 2003).

Due to the different distances to the isolated galaxies, our data cover different physical areas with different absolute magnitude limits (under the assumption that all faint galaxies lie at the same redshift as the primary galaxy). To deal with this situation we divided the isolated galaxy sample into three distance intervals, and derived the LF separately for each (see Fig. 14). Excluding the nearby group NGC 4697, our imaging of the other three groups covers a comparable area to that of the isolated galaxies. We note that in driving the LFs, we assume that the faint galaxies are at the same redshift as the primary galaxy. Spectra are required to determine the true redshift distribution of these galaxies. We find that the isolated galaxies and groups have similar luminosity functions. They all show a faint end slope of  $\sim -1.2$ , and a change in the slope around  $M_R \approx -18$ . Such features are fairly common across a range of environments (Flint 2001; Trentham & Tully 2002; Miles et al. 2004). We note that fossil groups (Jones et al. 2000) also reveal a similar luminosity function. This universality of isolated galaxy luminosity functions indicates that they

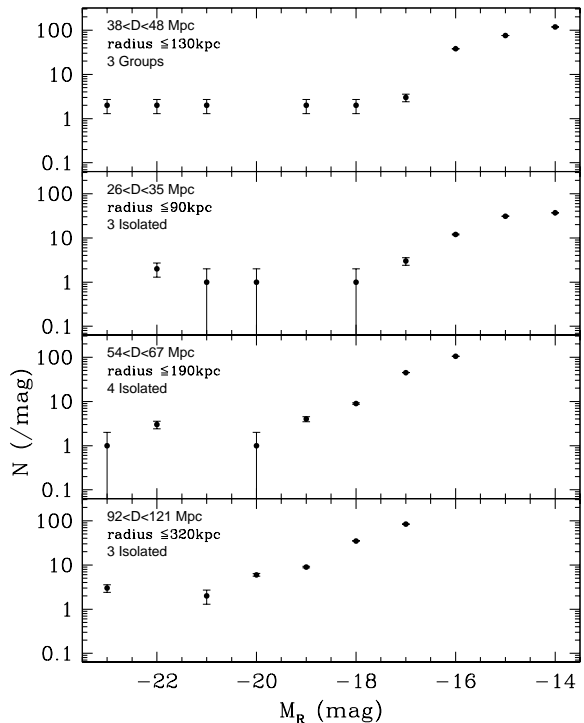


**Figure 14.** Differential luminosity function in the  $R$ -band for faint galaxies in the field of the ten isolated galaxies divided into three categories according to their distance. The top panel is the LF for three groups with distances comparable with the nearest isolated galaxies. Luminosity functions show a common faint end slope of about  $-1.2$ .

are not a useful tool in discriminating between competing ideas for the origin of isolated galaxies.

## 7.6 Space number density

To calculate the space number density of the detected faint galaxies surrounding the primary galaxy we divided the field into concentric annuli centred on each primary galaxy. The density measures in the outer annulii were corrected for the missing area with the largest correction being a factor of 2, i.e. 50% of the annulus was covered by the WFI field-of-view. The different magnitude limits in each field, determined by the exposure time, give rise to different background density levels.

In Figures 15 and 16, we display the space number density distribution of faint galaxies in the field of each primary galaxy. Seven out of ten isolated galaxies show almost constant density levels at all radii, indicating that the faint galaxies are mostly background objects and not associated with the isolated galaxies. The remaining three galaxies are NGC 2110, NGC 2865 and NGC 4240. Both NGC 2110 and NGC 4240 show a fairly continuous density decrease from the central region outwards. The outer most radial bin has a relatively high density suggesting that the background level has not been reached even at  $\sim 150$  kpc. NGC 2865 shows

**Figure 15.** Space number density of detected faint galaxies in the field of each primary galaxy. We show Poisson error bars. The horizontal dashed lines represent the estimated background density level. The name of each primary galaxy is indicated (N=NGC, M=MCG, and E=ESO). [See fig15to17.gif]

**Figure 16.** Same as Fig. 15. Note the different vertical scale for N4697. [See fig15to17.gif]

a sharp decline from a high central density to a background level at a radius of  $\sim 60$  kpc.

We note that these three galaxies are the closest in our sample, and for which we could detect lower luminosity dwarfs with magnitudes down to  $M_R \sim -13.5$ . The mean faint magnitude limit that could be detected for the other 7 isolated galaxies is  $M_R \sim -15.5$ . If we include only luminous dwarfs with  $M_R \lesssim -15.5$ , then these three galaxies show no central excess, giving similar space densities to those of other galaxies (Fig. 17). This indicates that the majority of dwarf galaxies associated with the isolated galaxies are less luminous than  $M_R \sim -15.5$ , while more luminous dwarfs are likely to be background objects.

In their study of the NGC 1132 environment, Mulchaey & Zabludoff (1999) measured a higher central density of dwarf galaxies, with magnitudes of  $17.22 < R < 19.22$ , than we have. From their density distribution we calculate the number of dwarfs within the central 80 kpc to be  $\sim 30$  galaxies. We identify only 8 galaxies within the same area. Our magnitude limit for the NGC 1132 field is  $R = 18.75$ . This magnitude difference is not enough to explain the density distribution difference between the two studies. Considering all detected objects down to their magnitude limit of  $R = 19.22$  and with ICCLASS parameters up to 0.95, we find 19 objects. This number of detected dwarf galaxies is still less than that found by Mulchaey & Zabludoff. This smaller number could be due to the incompleteness of our detections for objects fainter than  $R = 18.75$ . The background level in the outer region (i.e. distances  $> 100$  kpc) is consistent between the two studies.

As groups are distributed over a few megaparsecs, which is beyond our observed field-of-view, it is not surprising that the density levels remain high at all radii for our four group galaxies, i.e. none reach the background level. For IC 4320, after excluding its pair galaxy ESO509-G100, shows a constant density indicating no associated galaxies.

## 7.7 Comparison with fossil groups

Jones et al. (2003) defined a ‘fossil’ to be a giant isolated elliptical galaxy with group-like X-ray emission and luminosities of  $L_{X,bol} \geq 10^{42} h_{50}^{-2}$  erg s $^{-1}$ . Fossils are required to be  $\geq 2.0$   $R$  magnitudes brighter than the second bright-

**Figure 17.** Space number density of the detected dwarf galaxies in the fields of the three galaxies NGC 2110, NGC 2865 and NGC 4240. In this figure only luminous dwarfs of  $M_R \lesssim -15.5$  are included. The horizontal dashed lines represent the estimated background density level after this magnitude selection is applied. The luminous dwarfs are consistent with being background objects for all three galaxies. [See fig15to17.gif]

est galaxy in the system within half the projected virial radius. According to the hierarchical model of galaxy formation these elliptical galaxies are believed to be the end result of merging many small galaxies of a X-ray luminous group (Ponman et al. 1994; Jones, Ponman & Forbes 2000; Jones et al. 2003).

We have searched the literature for X-ray observations of our sample galaxies, finding only NGC 2865, NGC 3557 and NGC 4697 (O’Sullivan, Forbes & Ponman 2001), NGC 2110 (Bradt et al. 1978; Pfefferkorn, Boller & Rafanelli 2001), NGC 1132 (Mulchaey & Zabludoff 1999) and NGC 3528 and NGC 5266 (Horner & Goudfrooij 2004) to have published X-ray luminosities. Only NGC 1132 has an X-ray luminosity ( $L_X = 2.5 \times 10^{42} h_{50}^{-2}$  erg s $^{-1}$ ) that is comparable to a fossil.

In a study of 6 fossils, Jones et al. (2003) and Jones, Ponman & Forbes (2000) measured the  $R$  magnitude difference between the primary elliptical galaxy and the second brightest galaxy in the field to be  $\Delta R_{12} = 2.0 - 3.3$ . They considered all objects within  $\sim 600$  kpc of the primary galaxy. Excluding MCG-03-26-030, for the entire observed field around each of our isolated galaxies, we find  $\Delta R_{12} = 1.9 - 5.2$  and  $\Delta B_{12} = 2.3 - 4.8$ . If we use the maximum common radius for our sample of 116 kpc (which corresponds to the closest galaxy NGC 4240), we obtain similar values of  $\Delta R_{12} = 1.9 - 5.3$  and  $\Delta B_{12} = 2.3 - 5.4$ . The galaxy MCG-03-26-030 is the least isolated in our sample with a magnitude difference of 1.8 in the  $B$ -band. Thus our isolated galaxies have a similar, and some times even greater, luminosity isolation than ‘fossils’.

## 7.8 Possible formation scenarios

We now discuss the implications of our results in terms of various ‘straw-man scenarios’ for how isolated early-type galaxies may have formed. Our isolated galaxy images cover hundreds of square kiloparsecs of their surrounding fields. Using these images we are not only able to study the morphological structure of the galaxies themselves but also the magnitude and spatial distribution of the dwarf galaxies in their environments. Our selection criteria ensure that the galaxies are not currently undergoing a strong interaction with any other galaxy. The possible scenarios for isolated galaxies formation are:

1) *Clumpy collapse at an early epoch.* The early-type galaxy may have formed at a early epoch from the clumpy collapse or gaseous merger of many fragments. However the incidence of dust lanes, plumes and shells indicates that if the galaxy is very old, then it must have experienced a recent merger/accretion event. The low-density environment sample of Kuntschner et al. (2002) revealed much fine structure and young central ages indicating recent star formation – presumably induced by a recent merger/accretion. Thus if isolated galaxies formed a long time ago, some of them have undergone strong subsequent evolution.

2) *An equal-mass merger of two massive galaxies.* If we consider merging of two galaxies as the simple addition of their contents, without taking into account any star formation during the merger, then the merger of two progenitors of  $M_B \sim -20.25$  would produce an elliptical galaxy with magnitude of  $M_B \sim -21$ . The latter is a typical magnitude for our isolated galaxy sample. The merger of such galaxies

would be expected to lie on the Kormendy (1977) relation (Evstigneeva et al. 2004) as we have seen in Fig. 12. Furthermore the models of Bower et al. (1998) indicate that the merger of equal-mass galaxies will reproduce the slope and scatter of the CMR as we observe in Fig. 11. The 44% of isolated galaxies with dust would seem to require that at least one of the progenitors was a spiral galaxy. We note that in a detailed study of NGC 2865, Hau et al. (1999) concluded that it is the result of a merger involving one spiral and one early-type galaxy. The plume seen in NGC 1045 also requires the merger to have involved a spiral galaxy (e.g. Toomre & Toomre 1972). In the collisionless N-body simulations of Naab & Burkert (2003), mergers of two disks of equal-mass may produce a boxy elliptical, while higher mass-ratios may create low-luminosity, rapidly-rotating disky ellipticals. We find 11% (one galaxy; NGC 1045) to have boxy isophotes and 22% to have disky isophotes in our isolated galaxy sample. We conclude that the merger of two near-equal-mass galaxies, with at least one being a spiral, is a plausible scenario for several of our isolated galaxies.

3) *A large elliptical accretes several dwarf galaxies.* If the elliptical galaxy was initially located on the CMR, then the accretion of small dwarfs will not have a strong effect on its mass nor on its overall colour. A similar argument may apply to the Kormendy (1977) relation. However, we would expect low-luminosity dwarfs (with long dynamical friction timescales) to avoid accretion and be located close to the isolated galaxy. Such a trend is seen in the high central space density for three isolated galaxies (Fig. 15). Perhaps the main difficulty with this scenario is explaining the observed fine structure. In three galaxies, the morphological disturbance (e.g. plume, shells, dust lanes) is quite strong suggesting the accretion of a fairly large galaxy. For the remaining 6 isolated galaxies, this scenario can not be excluded.

4) *A group of galaxies collapses with its luminous galaxies merging together.* Such a scenario would give rise to a giant elliptical galaxy (Barnes 1989) with a magnitude comparable to the total magnitude of the original group. The magnitudes of our isolated galaxies are similar to poor groups but not typical of loose groups which have a total  $M_B \approx -22$ . The merged galaxies could explain the incidence of dust and other fine structure in our sample. However, we would again expect low-luminosity dwarfs to avoid the merger process, leaving a giant galaxy surrounded by a population of such dwarfs. In the case of a virialised X-ray group, its collapse is expected to produce an isolated early-type galaxy with an extended group-like X-ray emission (called a fossil) because the hot gas cooling time is very long. For our sample only NGC 1132, out of four galaxies with published X-ray luminosities, has a group-like X-ray emission. Thus most isolated early-type galaxies do not appear to be the result of a merged large group, but the possibility remains that they may be the product of a merged poor group.

## 8 CONCLUSION

In this paper we define a new sample of 36 early-type isolated galaxies. These galaxies are required to be at least 2  $B$ -band magnitudes brighter than the next brightest galaxy within 0.67 Mpc in the plane of the sky and recession velocity of 700

$\text{km s}^{-1}$ . Here we present wide-field imaging for 10 galaxies of this sample. We also include imaging of four group galaxies and an isolated galaxy pair for comparison. Our images cover a field-of-view of about  $30.6 \times 30.6$  arcmin, corresponding to an area of hundreds of square kiloparsecs surrounding each galaxy. From our CCD images we confirm the early-type morphology of our sample galaxies.

We used SExtractor to detect galaxies in the fields of the isolated galaxies. Assuming the galaxies in the field are located at the same redshift as the isolated galaxy, we estimate their photometric masses  $M$  and distances  $R$  from the isolated galaxy. Excluding all neighbouring galaxies with dynamical times less than a Hubble time, we calculated the quantity  $M/R^2$  which indicates the gravitational interaction force applied on the isolated galaxy by each galaxy in its local environment. Unlike the galaxies in groups, isolated galaxies are relatively gravitationally isolated with no neighbours having  $M/R^2 \gtrsim 4 \times 10^6 M_\odot/\text{kpc}^2$ .

A mean effective colour of  $(B-R)_e = 1.54 \pm 0.14$  is measured for our isolated galaxies which is similar to the colour of early-type galaxies in denser environments. Also, they are consistent with the slope and smaller scatter of the colour-magnitude relation for Coma cluster galaxies. This result suggests an early formation epoch for the bulk of stars in our isolated and group galaxies. However, there are also some morphological fine structures indicating recent merger/accretion events. The radial profile of the isophotal parameters, as well as the model-subtracted images reveal some fine structure such as plumes, dust, shells, disky and boxy structures in several isolated galaxies. About 44% of our isolated galaxies show such evidence of a past merger. The distribution of these different morphological features in our isolated galaxies is similar to that of luminous early-type galaxies in loose groups and clusters, suggesting a similar frequency of mergers and interactions.

Our isolated galaxies show a relation between the effective radius and the mean surface brightness within that radius (the Kormendy relation) which is consistent with that of luminous ellipticals in groups and clusters. This relation constrains the mass ratios of any merger progenitors to be near equal mass.

The galaxies in the fields of the isolated galaxies and the groups reveal similar luminosity functions with faint end slopes of  $\sim -1.2$  and a change in the slope at  $M_R \approx -18$ . This is similar to the luminosity functions obtained by other studies in a wide variety of environments.

We also briefly discuss possible formation scenarios for isolated galaxies. We conclude that the major merger of two massive galaxies could explain several of our sample galaxies. An alternative scenario of a collapsed poor group of a few galaxies is also possible, specifically to explain the observed high central density of dwarfs in the field of the isolated galaxy. The collapse of a large, virialized group does not appear to explain the most of our isolated galaxies. Mergers of many gaseous fragments or the accretion of several dwarfs by a large elliptical galaxy would not give rise to the observed fine structures seen in some of our isolated galaxies.

Future spectroscopic observations of the galaxies in the field of the isolated galaxies are needed to confirm their redshift, and hence whether they are associated with the isolated galaxies or not. High signal-to-noise spectra of the isolated galaxy itself will provide stellar populations and inter-

nal kinematics. This will be very useful to obtain a better idea about their star formation histories, and allow us to place additional constraints on their possible formation.

We wish to thank Dr. R. Proctor for his useful comments in the final revision of this paper. We are grateful to the supporting team at the Anglo Australian Observatory for their help during the observations. F.M.R acknowledges the 2-year scholarship funding from The Ministry of High Education in Egypt. F.M.R. also dedicates this work to the memory of her late teacher Prof. A.I. Gamal El Din (NRIAG, Egypt). We have used data from the Lyon-Meudon Extragalactic Database (LEDA) compiled by the LEDA team at the CRAL-Observatoire de Lyon (France). This research has made use of the NASA/IPAC Extragalactic Database, which is operated by the Jet Propulsion Laboratory, California Institute of Technology, under contract with the National Aeronautics and Space Administration.

## 9 REFERENCES

Aars C.E., Marcum P.M., Fanelli M.N., 2001, AJ, 122, 2923  
 Adams M., Jensen E., Stocke J.T., 1980, AJ, 85, 1010  
 Arp H.C., Madore B.F., 1987, A Catalogue of Southern Peculiar Galaxies and Associations. Cambridge Univ. Press, Cambridge  
 Amendola L., DiNella H., Montuori M., Sylos Labini F., 1997, *Fractals*, 5, 635  
 Balcells, M., 1997, ApJ, 486, 87  
 Balogh M.L., Morris S.L., 2000, MNRAS, 318, 703  
 Barnes J.E., 1989, Nat, 338, 123  
 Barnes J.E., Hernquist L., 1992, ARA&A, 30, 705  
 Baum W.A., 1959, PASP, 71, 106  
 Bender R., Döbereiner S., Möellenhoff C., 1988, A&AS, 74, 385  
 Bender R., Möellenhoff C., 1987, A&AS, 177, 71  
 Bender R., Surma P., Döbereiner S., Möellenhoff C., Madejsky R., 1989, A&AS, 217, 35  
 Bernardi M. et al., 2003, AJ, 125, 1882  
 Bertin E., Arnouts S., 1996, A&AS, 117, 393  
 Binney J., Petrou M., 1985, MNRAS, 214, 449  
 Binney J., Tremaine S., 1987, Galactic Dynamics. Princeton Univ. Press, Princeton, NJ  
 Blanton M.R. et al., 2001, AJ, 121, 2358  
 Blanton M.R. et al., 2003, ApJ, 592, 819  
 Bower R.G., Kodama T., Terlevich A., 1998, MNRAS, 299, 1193  
 Bower R.G., Lucey J.R., Ellis R.S., 1992, MNRAS, 254, 601  
 Bradt H.V., Burke B.F., Canizares C.R., Greenfield P.E., Kelley R.L., McClintock J.E., Koski A.T., van Paradijs J., 1978, ApJ, 226, 111  
 Capaccioli M., Caon N., D'Onofrio M., 1992, MNRAS, 259, 323  
 Christlein D., Zabludoff A., 2003, ApJ, 591, 764  
 Colbert J.W., Mulchaey J.S., Zabludoff A.I., 2001, AJ, 121, 808 (CMZ01)  
 de Carvalho R.R., Djorgovski S., 1992, ApJ, 389, L49  
 de Vaucouleurs G., de Vaucouleurs A., Corwin H.G., Buta R.J., Paturel G., Fouqu P., 1991, Third reference catalogue of bright galaxies. Springer, New York  
 Dressler A., 1980, ApJ, 236, 351  
 Drory N., Bender R., Feulner G., Hopp U., Maraston C., Snigula J., Hill G.J., 2003, ApJ, 595, 698  
 Ellis R.S., Smail I., Dressler A., Couch W.J., Oemler A., Butcher H., Sharples, R.M., 1997, ApJ, 483, 582  
 Evstigneeva E.A., de Carvalho R.R., Ribeiro A.L., Capelato H.V., 2004, MNRAS, 349, 1052  
 Flint K., 2001, PhD Thesis, UC Santa Cruz  
 Flint K., Bolte M., de Oliveira M., 2003, Ap&SS, 285, 191  
 Forbes D.A., 1991, MNRAS, 249, 779  
 Forbes D.A., Thomson R.C., 1992, MNRAS, 254, 723  
 Franx M., Illingworth G., Heckman T., 1989, AJ, 98, 538  
 Fujita Y., 2004, PASJ, 56, 29  
 Garcia A.M., 1993, A&AS, 100, 47  
 Girardi M., Mardirossian F., Marinoni C., Mezzetti M., Rigoni E., 2003, A&A, 410, 461  
 Gladders M.D., Lopez-Cruz O., Yee H.K.C., Kodama T., 1998, ApJ, 501, 571G  
 Graham A., Colless M., 1997, MNRAS, 287, 221  
 Goudfrooij P., de Jong T., Hansen L., Nørgaard-Nielsen H.U., 1994a, MNRAS, 271, 833  
 Goudfrooij P., Hansen L., Jørgensen H.E., Nørgaard-Nielsen H.U., de Jong T., van den Hoek L.B., 1994b, A&AS, 104, 179  
 Gunn J.E., Gott J.R., 1972, ApJ, 176, 1  
 Hamabe M., Kormendy J., 1987, in de Zeeuw T., ed., Proc. IAU Symp. 127, Structure and Dynamics of Elliptical Galaxies. Reidel, Dordrecht, p. 379  
 Hau G.K.T., Carter D., Balcells M., 1999, MNRAS, 306, 437  
 Hoessel J.G., Oegerle W.R., Schneider D.P., 1987, AJ, 94, 1111  
 Horner D., Goudfrooij P., 2004, submitted to AJ  
 Jedrzejewski R.I., 1987, MNRAS, 226, 747  
 Jones L.R., Ponman T.J., Forbes D.A., 2000, MNRAS, 312, 139.  
 Jones L.R., Ponman T.J., Horton A., Babul A., Ebeling H., Burke D.J., 2003, MNRAS, 343, 627  
 Karachentseva V.E., 1973, Comm. Spac. Ap. Obs. USSR, 8, 1  
 Khochfar S., Burkert A., 2003, ApJ, 597, 117  
 Khosroshahi H.G., Raychaudhury S., Ponman T.J., Miles T.A., Forbes D.A., 2004, MNRAS, 349, 527  
 Kodama T., Bower R.G., Bell E.F., 1999, MNRAS, 306, 561  
 Kodama T., 2001, A&SS, 276, 877  
 Kormendy J., 1977, ApJ, 218, 333  
 Kuntschner H., Smith R.J., Colless M., Davies R.L., Kaldare R., Vazdekis A., 2002, MNRAS, 337, 172  
 La Barbera F., Busarello G., Merluzzi P., Massarotti M., Capaccioli M., 2003, ApJ, 595, 127  
 Landolt A.U., 1992, AJ, 104, 340  
 Lauberts A., Valentijn E.A., 1989, The surface photometry catalogue of the ESO-Uppsala galaxies. European Southern Observatory (ESO), Garching  
 Lauer T.R., 1985, MNRAS, 216, 429  
 Merluzzi P., 1998, A&A, 338, 807  
 Miles T.A., Raychaudhury S., Forbes D.A., Goudfrooij P., Ponman T.J., 2004, MNRAS, submitted  
 Mobasher B., Colless M., Carter D., Poggianti B.M., Bridges T.J., Kranz K., Komiyama Y., Kashikawa N., Yagi M., Okamura S., 2003, ApJ, 587, 605  
 Moore B., Katz N., Lake G., Dressler A., Oemler A., 1996, Nat, 379, 613  
 Moore B., Lake G., Katz N., 1998, ApJ, 495, 139

Moore B., Lake G., Quinn Th., Stadel J., 1999, MNRAS, 304, 465

Mulchaey J.S., Zabludoff A.I., 1999, ApJ, 514, 133

Naab T., Burkert A., 2003, ApJ, 597, 893

Nieto J.-L., Bender R., 1989, A&A, 215, 266

O'Sullivan E., Forbes D.A., Ponman T.J., 2001, 328, 461

Peletier R.F., Davies R.L., Illingworth G.D., Davis L.E., Dawson M., 1990, AJ, 100, 1091

Pfefferkorn F., Boller Th., Rafanelli P., 2001, A&A, 368, 797

Ponman T.J., Allan D.J., Jones L.R., Merrifield M., McHardy I.M., Lehto H.J., Luppino G.A., 1994, Nat, 369, 462

Prugniel P., Heraudeau P., 1998, A&AS, 128, 299

Prugniel P., Simien F., 1997, A&A, 321, 111

Raychaudhury S., 1989, Nat, 342, 251

Raychaudhury S., 1990, BAAS, 22, 1331

Reduzzi L., Longhetti M., Rampazzo R., 1996, MNRAS, 282, 149 (RLR96)

Saucedo-Morales J., Biegling J., 2001, ApSSS, 277, 449

Schechter P., 1976, ApJ, 203, 297

Schlegel D.J., Finkbeiner D.P., Davis M., 1998, ApJ, 500, 525

Schweizer F., Seitzer P., Faber S.M., Burstein D., Dalle Ore C.M., Gonzalez J.J., 1990, ApJ, 364L, 33

Smith R.M., Martinez V.J., Graham M.J., 2003, preprint (astro-ph/0311599) (SMG03)

Soares D.S.L., de Souza R.E., de Carvalho R.R., Couto de Silva T.C., 1995, A&AS, 110, 371

Stanford S.A., Eisenhardt P.R.M., Dickinson M.E., 1995, ApJ, 450, 512

Stanford S.A., Eisenhardt P.R.M., Dickinson M.E., 1998, ApJ, 492, 461

Stocke J.T., Keeney B.A., Lewis A.D., Epps H.W., Schild R.E., 2004, AJ, 127, 1336

Terlevich A.I., Forbes D.A., 2002, MNRAS, 330, 547

Toomre A., Toomre J., 1972, ApJ, 178, 623

Trentham N., Hodgkin S., 2002, MNRAS, 333, 423

Trentham N., Tully R.B., 2002, MNRAS, 335, 712

Waddington I., Windhorst R.A., Cohen S.H., Dunlop J.S., Peacock J.A., Jimenez R., McLure R.J., Bunker A.J., Spinrad H., Dey A., Stern D., 2002, MNRAS, 336, 1342

Zabludoff A., & Mulchaey J., 2000, ApJ, 539, 136

Zepf S.E., Whitmore B.C., 1993, ApJ, 418, 72

Ziegler B.L., Saglia R.P., Bender R., Belloni P., Greggio L., Seitz S., 1999, A&A, 346, 13

Zwicky F. et al., 1957, Catalog of Galaxies & Clusters of Galaxies, Vol. 1-6, California Institute of technology, Pasadena

This figure "fig4\_1.gif" is available in "gif" format from:

<http://arxiv.org/ps/astro-ph/0408424v1>

This figure "fig5\_1.gif" is available in "gif" format from:

<http://arxiv.org/ps/astro-ph/0408424v1>

This figure "fig6\_1.gif" is available in "gif" format from:

<http://arxiv.org/ps/astro-ph/0408424v1>

This figure "fig4\_2.gif" is available in "gif" format from:

<http://arxiv.org/ps/astro-ph/0408424v1>

This figure "fig5\_2.gif" is available in "gif" format from:

<http://arxiv.org/ps/astro-ph/0408424v1>

This figure "fig6\_2.gif" is available in "gif" format from:

<http://arxiv.org/ps/astro-ph/0408424v1>

This figure "fig7.gif" is available in "gif" format from:

<http://arxiv.org/ps/astro-ph/0408424v1>

This figure "fig8.gif" is available in "gif" format from:

<http://arxiv.org/ps/astro-ph/0408424v1>

This figure "fig9.gif" is available in "gif" format from:

<http://arxiv.org/ps/astro-ph/0408424v1>

This figure "fig10.gif" is available in "gif" format from:

<http://arxiv.org/ps/astro-ph/0408424v1>

This figure "fig15.gif" is available in "gif" format from:

<http://arxiv.org/ps/astro-ph/0408424v1>

This figure "fig16.gif" is available in "gif" format from:

<http://arxiv.org/ps/astro-ph/0408424v1>

This figure "fig17.gif" is available in "gif" format from:

<http://arxiv.org/ps/astro-ph/0408424v1>